Effect of Hole Blockage Configurations on Film Cooling in Gas Turbine Components

Ke Tian[a], Jin Wang[a,b,*], Zhanxiu Chen[a], Li Yang[a], Guelailia Ahmed[c], Bengt Sundén[b]

[a]School of Energy and Environmental Engineering, Hebei University of Technology, Tianjin 300401, China
[b]Department of Energy Sciences, Division of Heat Transfer, Lund University, Lund SE-22100, Sweden
[c]University of Science and Technology of Oran, Oran-31000, Algeria
 wjwcn00@163.com

Usually, turbine blades operate under a harsh environmental condition. The inlet temperature of gas turbines increases with an improvement of the engine efficiency. Some cooling schemes are adopted to prevent the blades from thermal erosion of the hot mainstream. Film cooling technology is used widely and effectively in the blade cooling. In this paper, a comparison of hole blockage configurations was conducted by computational fluid dynamics. The results show that the film cooling effectiveness for a tetrahedral blockage case is higher than for other cases with various hemispherical blockages.

1. Introduction

With rapid development of the aerospace industry, initial temperature of gas turbines has been improved continually. In order to ensure the safe and efficient operation of gas turbines in the harsh environment, the cooling problem of the turbine blades has been paid more attention. Bogard and Thole (2012) compared the cooling efficiency of different hole configurations. They found that the fan-shaped hole has a higher averaged film effectiveness than that for the cylindrical hole. Moreover, the fly ash always deposits on the blade surface and inside the film hole, which impacts on the film cooling effectiveness. Bons et al. (2008) investigated the deposition of the turbine coupon. They found that the roughness size of the deposit experience a temporary lull in growth during the deposit evolution. Crosby (2007) investigated the effect of the particle size on deposition by using an accelerated deposition test facility.

In addition, fly ash can also deposit nearby the film cooling holes, even block them. Sundaram and Thole (2006) studied the effect of partial film-cooling hole blockage. They found that partially blocked holes will reduce film-cooling effectiveness. Ai et al. (2012) explored the particle deposition nearby the film cooling holes with the variation blowing ratios. And they found that increasing the blowing ratio will have a low deposition in the coolant path.

The purpose of this study is to investigate the effect of hemispherical and tetrahedral blockages on the film cooling effectiveness. Different blockage diameters and blocking positions are also analysed in this paper.

2. Description of Geometry

A three-dimensional (3D) geometry is used to coolant path investigate film cooling effectiveness by considering the effect of the hemispherical and tetrahedral blockage as shown in Figure 1. The diameter (d) of the film hole is 6 mm, and the hole with an inclination angle of 35° is located at x = 8d. The dimensions of the computational domain are 33d×10d×2d. The blockage configurations are located at the sidewall of the film hole.

Dimensions of blocking configuration are given in Table 1. It shows three diameters (d) of the hemispherical blockage configurations and the blocking ratios (BR). And there are three distances (e) from the outlet of the film hole listed in the table. And the blockage ratio is calculated by dividing the maximum cross-sectional area

of the blockage configuration by the section area of the round hole. Case-7 is tetrahedral blockage with a similar blockage ratio with Case-2.
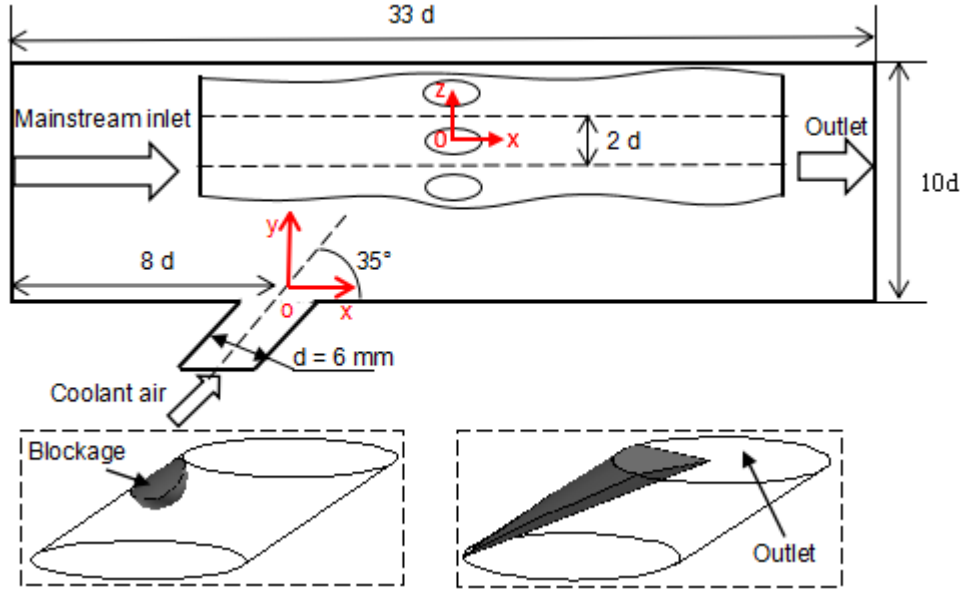

Figure 1: Sketch of computational domain

Table 1: Dimensions of blocking configuration

Item	Diameter (d), mm	Distance (e), mm	Blockage ratio (BR)
Case-0	No blockage	No blockage	0 %
Case-1	2	/	Hemisphere: 5 %
Case-2	4	/	Hemisphere: 20 %
Case-3	6	/	Hemisphere: 37 %
Case-4	/	1	Hemisphere: 5 %
Case-5	/	2	Hemisphere: 5 %
Case-6	/	6	Hemisphere: 5 %
Case-7	/	/	Tetrahedron: 21 %

3. Governing equations

For this paper, the governing equations of mass, momentum, energy, the turbulent kinetic energy and the turbulent dissipation rate are shown as follows:

$$\frac{\partial}{\partial x_i}(\rho u_i) = S_m \tag{1}$$

$$\frac{\partial}{\partial x_i}(\rho u_i u_j) = \rho \bar{g}_j - \frac{\partial P}{\partial x_j} + \frac{\partial}{\partial x_i}(\tau_{ij} - \rho \overline{u_i' u_j'}) + F_j \tag{2}$$

$$\frac{\partial}{\partial x_i}(\rho c_p u_i T) = \frac{\partial}{\partial x_i}\left(\lambda \frac{\partial T}{\partial x_i} - \rho c_p \overline{u_i' T'}\right) + \left|\mu \Phi + S_h\right| \tag{3}$$

$$\frac{\partial}{\partial x_i}(\rho u_i k) = \frac{\partial}{\partial x_i}\left(\left(\mu + \frac{\mu_t}{\sigma_k}\right)\frac{\partial k}{\partial x_i}\right) + G_k - \rho \varepsilon \tag{4}$$

$$\frac{\partial}{\partial x_i}(\rho u_i \varepsilon) = \frac{\partial}{\partial x_i}\left(\left(\mu + \frac{\mu_t}{\sigma_z}\right)\frac{\partial \varepsilon}{\partial x_i}\right) + \rho C_1 S\varepsilon - \rho C_2 \frac{\varepsilon^2}{k + \sqrt{v\varepsilon}} + C_1 \frac{\varepsilon}{k}C_{3\varepsilon}G_b + S_\varepsilon \qquad (5)$$

More details can be found in (Wilcox, 2006).

4. Boundary conditions

Boundary conditions are shown in Table 2. Both the mainstream and the coolant flow are assumed to be air and the temperature values of the inlets are 338 K and 300 K. The mainstream velocity is 25 m/s. The coolant air velocity is 13.3 m/s and the corresponding blowing ratio (M) is 0.53. The blowing ratio is defined as M=$(\rho u)_c/(\rho u)_g$, where the subscript c and g are represent the coolant flow and the mainstream gas.

Table 2: Boundary conditions

Zone	Type	Value
Mainstream	Velocity-inlet	25 m/s, 338 K
Coolant air	Velocity-inlet	M = 0.53, 300 K
Outlet	Pressure-outlet	101325 Pa
Side walls	Symmetry	/
Other walls	No-slip	/

5. Meshes

Both structured and unstructured grids are used by a multi-block topology as shown in Figure 2. The nearest wall cell had a value of y+ = 2.6.
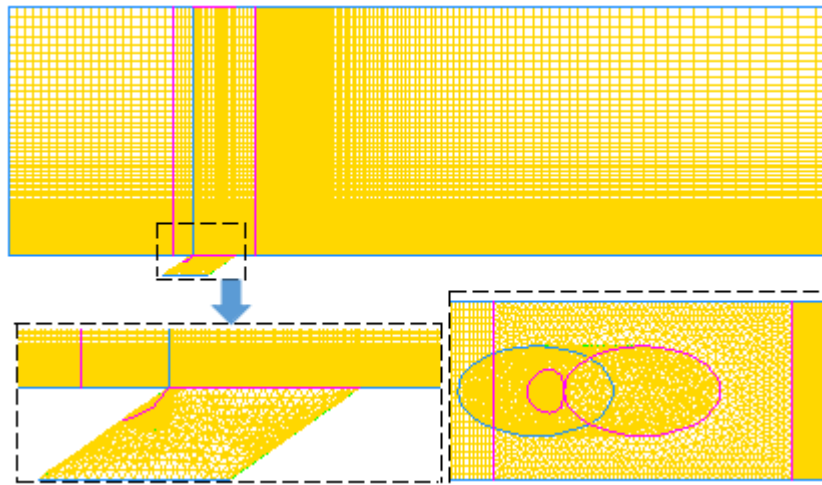

Figure 2: Grid meshes

6. Convergence and Model validation

Three different meshes (0.32M, 0.84 M and 1.20M) were used to investigate the grid independence as shown in Figure 3. There is a big difference between the simulated results for 0.32 and 0.84 M cells. However, the cooling effectiveness for the case with the 1.20 M cells has a similar trend with for the case with the 0.84 million cells. Therefore, the case with the 0.84 M cells was used in this study. Typically, in order to achieve stable convergences, 2,000 – 3,000 iterations are needed, which takes about 6 h on a computer with an E5-2680 processor of 2.7 GHz.

Software ANSYS FLUENT 16.2 was used in this study. In order to validate the calculation method, the average cooling effectiveness based on two kinds of k-ε turbulence models were compared to the results in Huang et al. (2014). It has a similar trend with the results in the other results, so the Realizable k- ε turbulence model was used as shown in Figure 3.
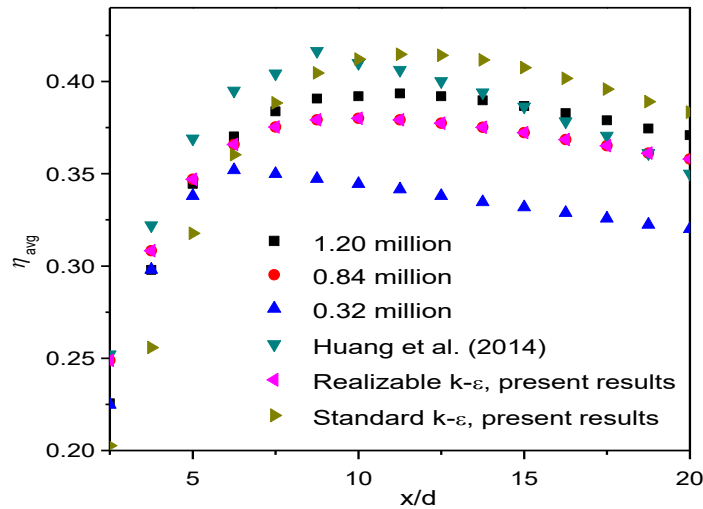
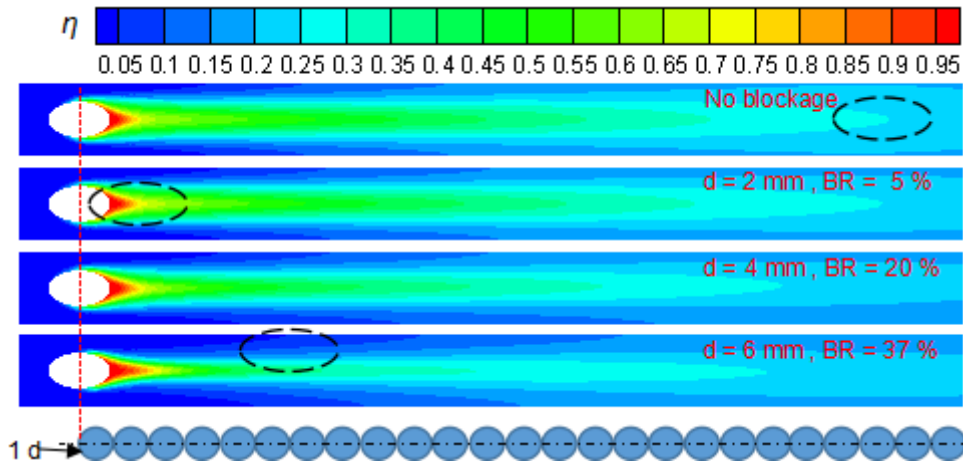*Figure 3: Grid independence and model validation*

7. Results and Discussion

Figure 4: Wall film cooling effectiveness for different hemispherical blockage cases.

The film cooling effectiveness η is defined as $\eta=(T_g-T_{aw})/(T_g-T_c)$, and the dimensionless temperature θ is defined as $\theta=(T_g-T_{la})/(T_g-T_c)$. T_g, T_{aw}, T_c, and T_{la} are the mainstream gas temperature, the adiabatic wall temperature, the coolant flow temperature and the local air temperature, respectively.

The film cooling distributions for different blockage cases are shown in Figure 4. The film cooling effectiveness at various positions are quite different as shown in the dotted circles. With increasing the blockage ratio by changing the diameters of the hemispherical blockage, the coverage area of the coolant air is reduced. Therefore, the lateral film cooling effectiveness decreases significantly.

Figure 5 shows the dimensionless temperature along the centerline of the wall surface. The outlet area of the film hole is reduced for the case with a large blockage ratio, and the coolant air is pushed into the wall. The dimensionless temperature downstream the wall increases first and then decreases.

Film cooling effectiveness for both hemispherical and tetrahedral blockages is shown in Figure 6. It is found that the tetrahedral configuration case shows a higher cooling effectiveness than the hemispherical case. Although two different configurations have the approaching blockage ratios, the largest cross-sectional area of the hemispherical blockage appears far away from the outlet of the film hole. Therefore, when the coolant flow bypasses the hemispherical blockage, the coolant air occupies the space behind the blockage. The blockage position weakens the adhesion force from the coolant to the wall. Compared with the hemispherical blockage case, the tetrahedral configuration obtains a stronger adhesion force and the uplift of the coolant flow is weakened. It is concluded that the tetrahedral blockage increases the film cooling effectiveness, while the hemispherical blockage decreases the film cooling effectiveness.
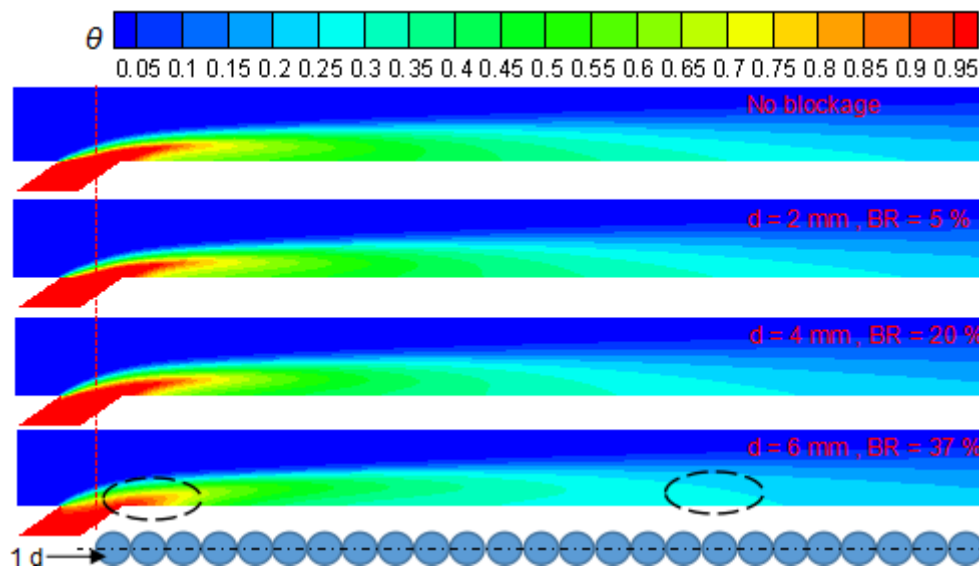
*Figure 5: D*imensionless temperature *on the middle section downstream the wall.*
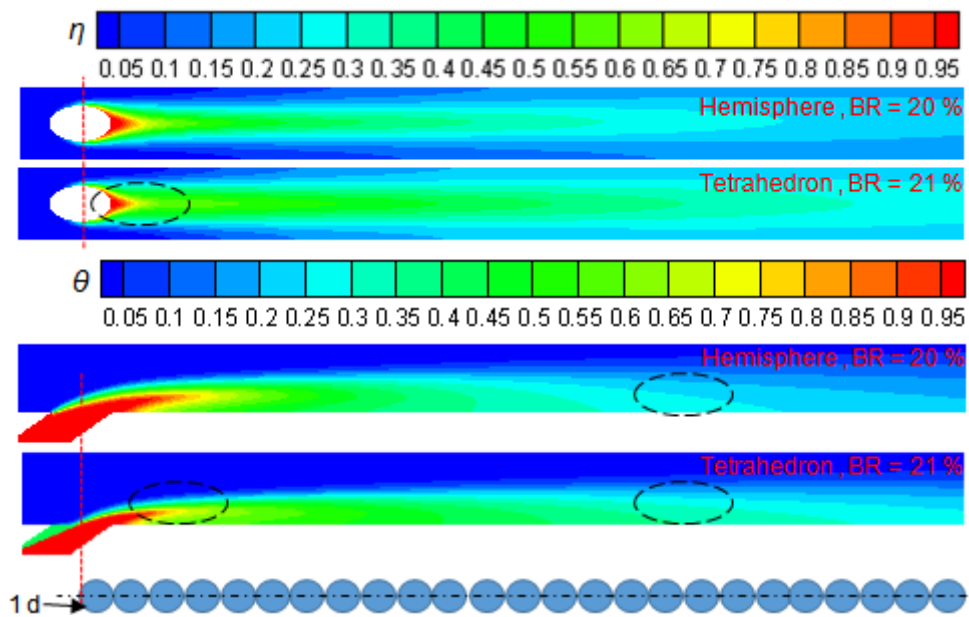

Figure 6: Film cooling effectiveness for the hemispherical and tetrahedral blockage cases.

Figure 7 shows the film cooling effectiveness downstream the wall for different blockage cases. As described earlier, the high blockage ratio case (BR = 37 %) has a high film cooling effectiveness nearby the hole, but it decreases faster than the low blockage ratio case (BR = 5 %). Distance has little influence on the film cooling effectiveness, except the case tangent with the outlet of the gas film hole (d = 2 mm, e = 1 mm). When the blockage nearby the outlet of the hole such as the Case-S1, the section area of the round hole will decrease. For this reason, the film cooling effectiveness of the Case-S1 is lower than that of other two cases. In addition, the film cooling effectiveness is enhanced when the tetrahedral blockage is located at the hole outlet.
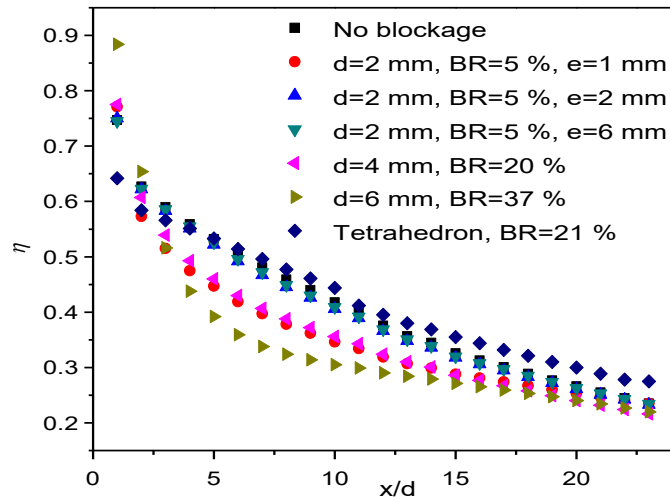
Figure 7: Film cooling effectiveness downstream the wall for different hemisphere and tetrahedron blockage cases.

8. Conclusions

Numerical simulations were performed to investigate the effects of different diameters, distances and blockage configurations on film cooling characteristics. For the same hemispherical configurations, the results show that the film cooling effectiveness decreases with increasing the diameter of the blockage configuration. For the same blocking ratio, different distances from the outlet of the film hole have little influence on the film cooling effectiveness. Finally, the case with a tetrahedral blockage configuration enhances the film cooling effectiveness compared to the other cases with various hemispherical blockages.

References

Ai W., Murray N., Fletcher T.H., Harding S., Lewis S., Bons J.P., 2012, Deposition Near Film Cooling Holes on a High Pressure Turbine Vane, ASME Turbo Expo 2008: Power for Land, Sea, and Air, 134, 825-835.

Bogard D.G., Thole K.A., 2012, Gas Turbine Film Cooling, Journal of Propulsion & Power, 22, 249-270.

Bons J.P., Wammack J.E., Crosby J., Fletcher D., Fletcher T.H., 2008, Evolution of Surface Deposits on a High Pressure Turbine Blade: Part II — Convective Heat Transfer, Journal of Turbomachinery, 130, 1075-1082.

Crosby J.M., 2007, Particle Size, Gas Temperature, and Impingement Cooling Effects on High Pressure Turbine Deposition in Land Based Gas Turbines from Various Synfuels. MSD Thesis, BYU, Provo, US.

Huang K.N., Zhang J.Z., Wen G., 2014, Effect of Partial Blockage Inside Film Hole on Film Cooling Characteristics, Journal of Aerospace Power, 29, 1330-1338.

Sundaram N., Thole K.A., 2006, Effects of Surface Deposition, Hole Blockage, and TBC Spallation on Vane Endwall Film-Cooling, ASME Turbo Expo 2006: Power for Land, Sea, and Air, 129, Barcelona, Spain, 599-607, doi:10.1115/gt2006-90379.

Wilcox D.C., 2006, Turbulence Modeling for CFD, DCW Industries Inc., California, USA, 522 ps, ISBN: 987-1-928729-08-2.